The Astrophysical Journal, 763:137 (12pp), 2013 February 1 doi:10.1088/0004-637X/763/2/137

ROTATION RATES OF CORONAL HOLES AND THEIR PROBABLE ANCHORING DEPTHS

K. M. Hiremath and M. Hegde
Indian Institute of Astrophysics, Bangalore, India; hiremath@iiap.res.in
Received 2011 October 5; accepted 2012 December 4; published 2013 January 17

ABSTRACT

From 2001–2008, we use full-disk, *SOHO*/EIT 195 Å calibrated images to determine latitudinal and day-to-day variations of the rotation rates of coronal holes (CHs). We estimate the weighted average of heliographic coordinates such as latitude and longitude from the central meridian on the observed solar disk. For different latitude zones between 40° north and 40° south, we compute rotation rates and find that, irrespective of their area, the number of days observed on the solar disk, and their latitudes, CHs rotate rigidly. Combined for all the latitude zones, we also find that CHs rotate rigidly during their evolution history. In addition, for all latitude zones, CHs follow a rigid body rotation law during their first appearance. Interestingly, the average first rotation rate (∼438 nHz) of CHs, computed from their first appearance on the solar disk, matches the rotation rate of the solar interior only below the tachocline.

Key words: Sun: atmosphere – Sun: corona – Sun: helioseismology – Sun: interior – Sun: rotation – Sun: UV radiation

Online-only material: color figures

1. INTRODUCTION

Solar coronal holes (CHs) are large regions in the solar corona with low-density plasma (Krieger et al. 1973; Neupert & Pizzo, 1974; Nolte et al. 1976; Zirker 1977; Cranmer 2009 and references therein; Wang 2009) and unipolar magnetic field structures (Harvey & Sheeley 1979; Harvey et al. 1982) distinguished as dark features in EUV and X-ray wavelength regimes. During the solar maximum, CHs are distributed at all latitudes, while at solar minimum, CHs mainly occur near the polar regions (Madjarska & Wiegelmann 2009). In addition to sunspot activity and magnetic activity phenomena that strongly influence the Earth's climate (Hiremath 2009 and references therein), there is increasing evidence that, on short timescales, occurrences of solar CHs trigger responses in Earth's upper atmosphere and magnetosphere (Soon et al. 2000; Lei et al. 2008; Shugai et al. 2009; Sojka et al. 2009; Choi et al. 2009; Ram et al. 2010; Krista 2011; Verbanac et al. 2011).

The physics of solar cycle and activity phenomena is not well understood (Hiremath 2010a, 2010b and references therein).

In order to understand the solar cycle and activity phenomena, an understanding of the rotational structure of the solar interior and the surface are necessary. The rotation rate of the interior and the surface are coupled with the rotation rate of the solar atmosphere, especially the corona. Although there is a general consensus regarding the interior rotation as inferred from helioseismology (Dalsgaard & Schou 1988; Thompson et al. 1996, 2003 and references therein; Antia et al. 1998; Howe 2009; Antia & Basu 2010), surface rotation rates as derived from sunspots (Newton & Nunn 1951; Howard et al. 1984; Balthasar et al. 1986; Shivaraman et al. 1993; Javaraiah 2003), Doppler velocity (Howard & Harvey 1970; Howard & La Bonte 1980; Ulrich et al. 1988; Snodgrass & Ulrich 1990), and magnetic activity features (Wilcox & Howard 1970; Snodgrass 1983; Komm et al. 1993), there is no such consensus (see also Li et al. 2012) on the magnitude and form of the rotation law for features in the corona.

For example, by using CHs as tracers (Wagner 1975, 1976; Timothy & Krieger 1975; Bohlin 1977) and large-scale coronal structures (Hansen et al. 1969; Parker et al. 1982; Fisher & Sime 1984; Hoeksema 1984; Wang et al. 1988; Weber et al. 1999; Weber & Sturrock 2002), previous studies show that the corona rotates rigidly, while other studies (Shelke & Pande 1985; Obridko & Shelting 1989; Navarro-Peralta & Sanchez-Ibarra 1994; Insley et al. 1995) indicate differential rotation. In addition to using CHs as tracers, X-ray bright points (Chandra et al. 2010; Kariyappa 2008; Hara 2009), coronal bright points (Karachik et al. 2006; Brajša et al. 2004; Wöhl et al. 2010), and *SOHO*/LASCO images have been used for the computation of rotation rates and yield a differentially rotating corona. Recent studies using radio images at 17 GHz (Chandra et al. 2009) and synoptic observations of the O VI 1032 Å spectral line from the *SOHO*/UVCS telescope (Mancuso & Giordano 2011), however, suggest that the corona rotates rigidly. As part of an ISRO (Indian Space Research Organization) funded project, the present study utilizes *SOHO*/EIT 195 Å calibrated images for understanding the following four objectives: (1) checking for latitudinal dependency of the rotation rates of CHs, (2) studying the rotation rates of CHs during their first appearance on the observed disk, (3) irrespective of their latitude, studying the day-to-day variation of the rotation rates of CHs, and (4) estimating the probable anchoring depths of CHs. In Section 2, we present the data used and method of analysis, and the results of that analysis in Section 3. In Section 4, we discuss the cause of the rigid body rotation rate of the CHs and conclude with estimations of their probable anchoring depths.

2. DATA AND ANALYSIS

From 2001–2008, we use full-disk *SOHO*/EIT images (Delaboudiniére et al. 1995) that have a resolution of 2.6 arcsec pixel^{-1} in a bandpass around 195 Å to detect CHs. The period studied includes both intense activity near solar maximum and the descent of solar activity parameters such as 10.7 cm flux to values of ∼half of their values around that maximum. The obtained images are in FITS format and individual pixels are in units of data number (DN). DN is defined as the output of the instrument electronics that corresponds to the incident photon signal converted into charge within each CCD pixel (Madjarska & Wiegelmann 2009).

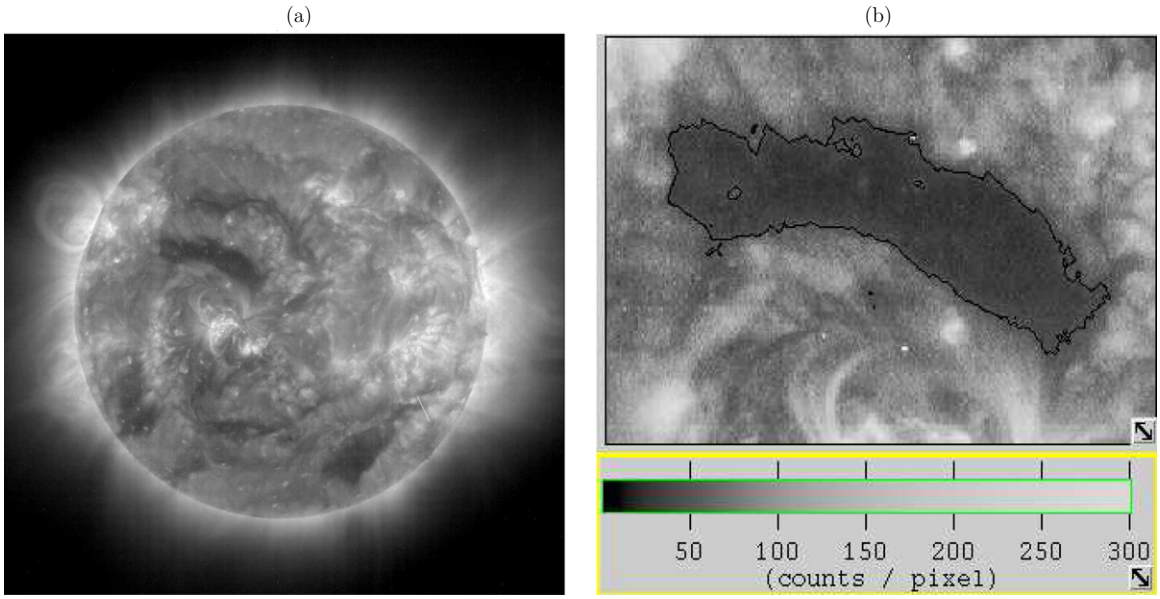

Figure 1. Panel (a) shows a full-disk *SOHO*/EIT 195 Å image of 2001 January 1, 00:24:11 UT with CHs (in the northeastern hemisphere and close to center) and panel (b) illustrates a threshold DN contour map of the same CHs.

(A color version of this figure is available in the online journal.)

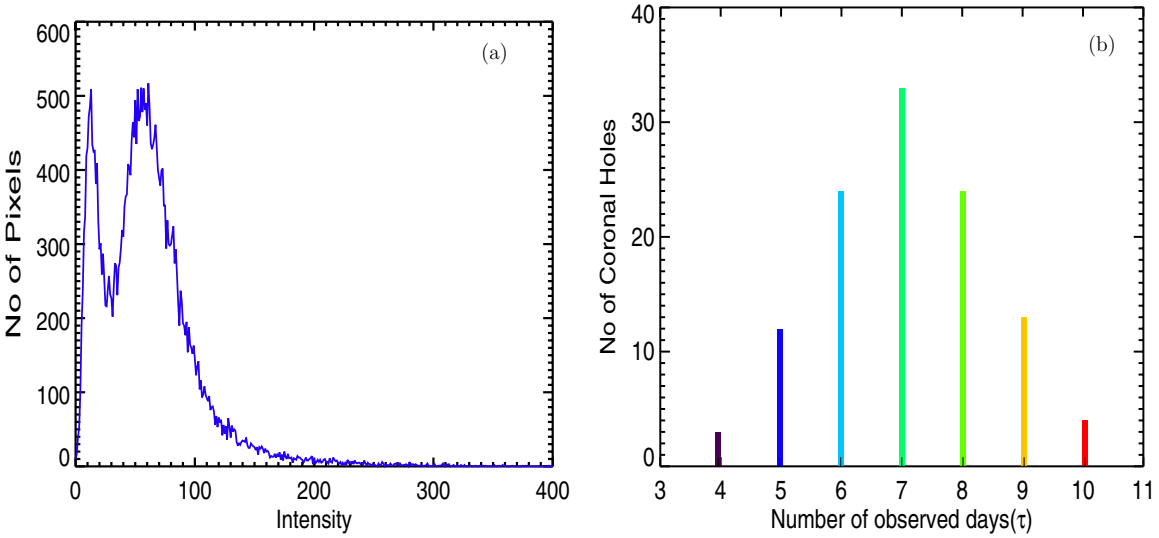

Figure 2. Panel (a) illustrates a DN histogram of a typical coronal hole. Panel (b) illustrates the total number of CHs for the number of days (τ) observed on the solar disk.

(A color version of this figure is available in the online journal.)

We consider CHs that appear and disappear between 40° north and 40° south latitude of the visible solar hemisphere. Using the SolarSoft eit_prep routine (Freeland & Handy 1998), we background subtracted, flat-fielded, degridded, and normalized the images. As this calibration involves exposure normalization of the images, henceforth a unit of DN is DN s^{-1}. We used the occurrence dates and position of CH from the http://www.spaceweather.com Web site. As this Web site is not designed for scientific use, we use readily available occurrence dates of CH only. By using the approximate positions (heliographic coordinates) of CHs from this Web site, we separate a region from the *SOHO*/EIT images for further analysis and extraction of relevant physical parameters, as described below. A CH is also confirmed if it has a bimodal distribution in the intensity histogram.

In order to extract physical parameters of CHs from the Extreme ultraviolet Imaging Telescope (EIT) images, we use FV interactive FITS file editor (http://heasarc.gsfc.nasa.gov/docs/software/ftools/fv/). Depending upon the shape of the CH, from the FV editor, a circle or an ellipse is drawn covering the whole region of the CH, and average DN (intensity), set as a threshold for detecting the boundary of a CH, is computed for detecting the boundary (private communications with Prof. Aschwanden). Similar to Karachik & Pevtsov (2011), the threshold is modified for some of the CHs to match the visually estimated boundary. This method yields results consistent with the previous intensity histogram methods (Krista & Gallagher 2009; Krista 2011; de Toma 2011 and references therein). After determining the boundary of CHs, we employ SolarSoft coordinate routines to compute the central meridian distance (l_i)

Table 1
Computation of Heliographic Coordinates with Different Weights in Equation (1)

	CH1		CH2		CH3	
Weights	Longitude (deg)	Latitude (deg)	Longitude (deg)	Latitude (deg)	Longitude (deg)	Latitude (deg)
DN	−8.374	12.604	8.352	−11.727	4.011	−3.898
1/DN	−8.445	12.836	8.637	−12.682	3.818	−3.996
Average	−8.400	12.715	8.489	−12.206	3.917	−3.945

(heliographic longitude from the central meridian) and latitude (θ_i) of individual pixels within the CH.

Figure 1(a) shows a full disk, solar image with a typical CH close to the center and in the northeast quadrant, while Figure 1(b) represents the same CH with a threshold DN contour map. In Figure 2(a), the DN histogram of the CH is presented. The bimodal distribution in the histogram confirms the DN values in the CH region (Krista & Gallagher 2009; Krista 2011). We sum the total number of pixels and total DN within the CH boundary, which in turn allows us to compute average heliographic coordinates such as latitude (θ) and central meridian distance (L) of CH as follows:

$$\theta = \frac{\sum_{i=1}^{n} \theta_i * \mathrm{DN}_i}{\sum_{i=1}^{n} \mathrm{DN}_i} \quad L = \frac{\sum_{i=1}^{n} l_i * \mathrm{DN}_i}{\sum_{i=1}^{n} \mathrm{DN}_i}, \tag{1}$$

where θ_i, l_i, and DN_i (for $i = 1, n$, n is number of pixels) are the latitude, the central meridian distance, and DN values of individual pixels, respectively. This method of finding the average heliographic coordinates of CHs is equivalent to a method in physics of finding the center of mass of an arbitrary geometrical shape.

As the average heliographic coordinates of CHs are weighted by the intensity (DN counts) of the relevant pixel, one can argue that more weight is given to brighter pixels. However, this argument cannot be valid in this case as the intensity is also weighted in the denominator (see above Equation (1)) and, hence, whatever higher weights given to the brighter pixels in the numerator are also equally compensated by the higher weights in the denominator. We also check with another weighting that emphasizes areas darker than the image mean (i.e., $(\sum_{i=1}^{n} \mathrm{DN}_i/N) - \mathrm{DN}_i)$) and obtain the same results of the average heliographic coordinates, suggesting that the weighted average used in Equation (1) is correct and is not biased toward the brighter pixels.

For computation of the heliographic coordinates of CHs, we also use weights with the inverse of DN (1/DN) and no weights at all (i.e., simple averages) in Equation (1). The results for three typical CHs are presented in Table 1. The negative sign for the longitude indicates the CHs that are on the eastern side of the central meridian, and the negative sign for the latitudes indicates the CHs that are in the southern hemisphere. One can notice from this table that irrespective of weighted and non-weighted averaging, computed heliographic coordinates of CHs are nearly the same.

Following the previous method (Hiremath 2002) of the computation of sunspot rotation rates, daily siderial rotation rates Ω_j of the CH are computed as follows:

$$\Omega_j = \frac{(L_{j+1} - L_j)}{(t_{j+1} - t_j)} + \delta\Omega, \tag{2}$$

where L_j, L_{j+1} are average longitudes of the CH for the two consecutive days t_j and t_{j+1}, respectively, $j = 1, 2, \ldots, n-1$, n is the number of days of appearance of CHs on the visible solar disk, and $\delta\Omega$ is a correction factor for the orbital motion of the Earth around the Sun. Strictly speaking, this correction factor is due to orbital motion of the *Solar and Heliospheric Observatory* (*SOHO*) spacecraft around the Sun. Compared to the distance between the Sun and Earth, the distance between the *SOHO* satellite and the Earth is very small and, hence, the orbital distances of the Earth and the satellite are almost the same and the correction factor $\delta\Omega$ is $\sim$1 deg day^{-1}. For the present work, this approximation is sufficient. However, if one wants to find the long-term ($\sim$11 yr) variation of rotation rates, the correction factor $\delta\Omega$ should be computed accurately (Roša et al. 1995; Wittmann 1996; Brajša et al. 2002). From the first- and second-day appearances of a CH, one can compute the rotation rate Ω_1 that we call the *first rotation rate*. Similarly, for other successive days, rotation rates Ω_2, Ω_3, etc., are computed. For each computed rotation rate of CHs, the respective latitude is assigned as the average of two latitudes corresponding to the two longitudes. We also compute the standard deviation and error bars of the average heliographic coordinates and rotation rates. Henceforth, computation of rotation rates of CHs from Equation (2) is called the *First Method*.

3. RESULTS

We follow the following criteria in selecting CH data: (1) in order to avoid projection effects (especially CHs near both the eastern and the western limbs), we consider only the CHs that emerge within 65° central meridian distance; (2) the CH must be compact, independent, and not elongated in latitude; and (3) during its passage across the solar disk, it should not merge with other CHs. For the period of observations from 2001 to 2008, a total of 113 CHs satisfy these criteria. We define the term τ of a CH as total number of days observed on the same part of the solar disk satisfying the afore-mentioned criteria. If we assume that CHs decay due to magnetic diffusion only, as the dimension L of a CH is very large (from Section 3.1, one can note that area A is $\sim 10^{20}$ cm^2), magnetic diffusion timescale τ ($(L^2/\eta) \sim (A/\pi\eta)$, where η is magnetic diffusivity and area A of a CH is assumed to be a circle; magnetic diffusivity in the corona is considered to be $\sim 10^{13}$ cm^2 s^{-1}; Krista 2011; Krista et al. 2011) is estimated to be $\sim$2 months. Hence, there is a possibility that CHs might have reappeared on the visible disk and might have diffused in the solar atmosphere. Hence, the *actual lifespan* of a CH must be of longer duration. In Figure 2(b), for different τ, we present the occurrence number of CH considered for this study.

During their evolutionary passage over the solar disk, we compute rotation rates and assign respective latitudes. If a CH exists for n days, then its τ is n days and the total number of rotation rates is $(n-1)$. The rotation rates of non-recurrent CHs that appear and disappear on the visible disk are computed. According to the above definition, and in the present data set (see Figure 2(b)), we find 4 CHs that appear for 10 days, 13 CHs for 9 days, and so on. Integrated over all latitudes and in both the hemispheres, we determine a total of 683 rotation rates.

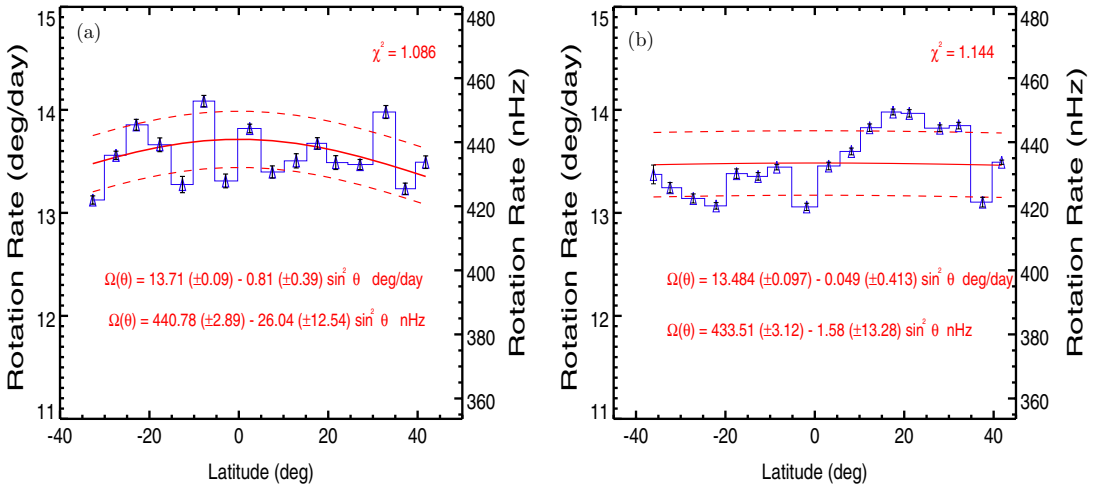

Figure 3. For different latitudes, the rotation rates of coronal holes computed from the first method (see Section 2). Panel (a) illustrates the rotation rates of CHs that occur between 65° east and west of the central meridian distance, and panel (b) illustrates the rotation rates of CHs that occur between 45° east and west of the central meridian distance. In both panels, the blue bar plot represents the observed rotation rates, the red dashed lines represent the one standard deviation (which is computed from all the data points) error bands, and the red continuous line represents a least-square fit of the form $\Omega(\theta) = \Omega_0 + \Omega_d \sin^2\theta$ to the observed values. $\Omega(\theta)$ is the observed CH rotation rate, θ is the latitude, and Ω_0 and Ω_d are the constant coefficients determined from the least square fit. χ^2 is a measure of goodness of fit.

(A color version of this figure is available in the online journal.)

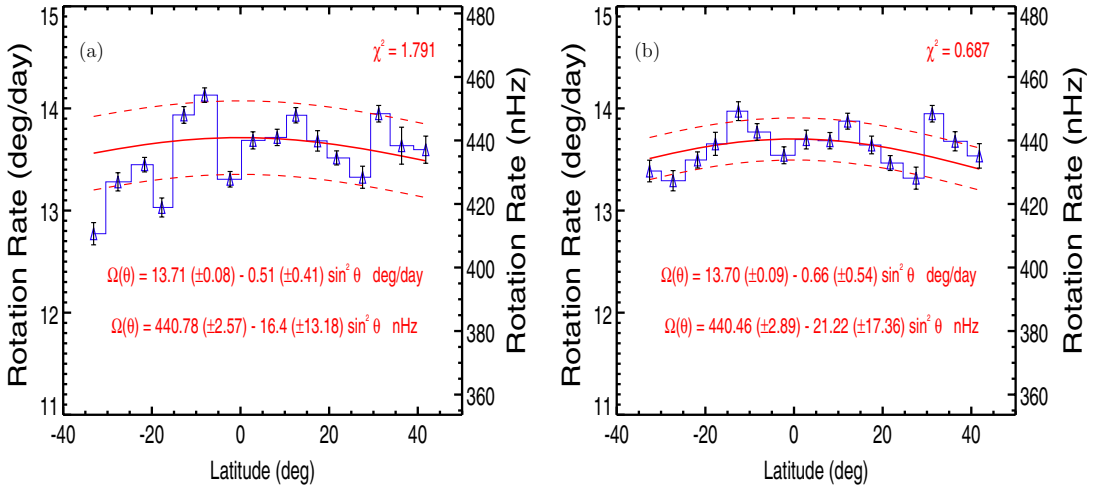

Figure 4. For different latitudes, the rotation rates of coronal holes computed from the second method (see Section 3.1). Panel (a) illustrates the rotation rates of CHs that occur between 65° east and west of the central meridian distance, and panel (b) illustrates the rotation rates of CHs that occur between 45° east and west of the central meridian distance. In both panels, the blue bar plot represents the observed rotation rates, the red dashed lines represent one standard deviation (which is computed from all the data points) error bands, and the red continuous line represents a least-square fit of the form $\Omega(\theta) = \Omega_0 + \Omega_d \sin^2\theta$ to the observed values. $\Omega(\theta)$ is the observed CH rotation rate, θ is the latitude, and Ω_0 and Ω_d are the constant coefficients determined from the least-square fit. χ^2 is a measure of goodness of fit.

(A color version of this figure is available in the online journal.)

3.1. Average Rotation Rates: Variations With Respect to Latitude and Area

During their passage over the solar visible disk, the daily rotation rates of CHs are computed. In both hemispheres, for each latitude bin of 5°, we collect rotation rates and compute average rotation rates with their respective standard deviations σ and the errors ($\sigma/\sqrt{N}$, where N is the number of rotation rates). We present the results in Figure 3(a), which illustrates the variation of average rotation rates of the CHs for different latitudes. To be on the safer side from the projectional effects, we also compute the *average rotation rates* of CHs that emerge within 45° central meridian distances and are illustrated in Figure 3(b). For the sake of comparison with helioseismic inferred rotation rates, in both the plots we include a frequency scale on the right-hand side of the vertical axis. For different latitude bins, the observed rotation rates are subjected to a least-square fit of the form $\Omega(\theta) = \Omega_0 + \Omega_d \sin^2\theta$ (where θ is the latitude and Ω_0 and Ω_d are constant coefficients to be determined).

There is every possibility that the errors from determining the centers of CHs may propagate to the rotation rates and, hence, rotation rates determined from the first method may effectively enhance the error in the second coefficient (Ω_d), yielding rigid body rotation rates of CHs. Moreover, the drawback of the first method is also reflected in Figure 3(b), where unlikely asymmetrical rotation profile in both hemispheres is obtained. In order to minimize such propagating errors in the rotation rates of CHs determined by the first method, we compute rotation rates of CHs in the following way, defined as the *second method*. In this method, as suggested by the referee, we fit all the daily centroid positions of the individual CHs by a first degree polynomial, with the computed second coefficient (slope) representing the rotation rate. For

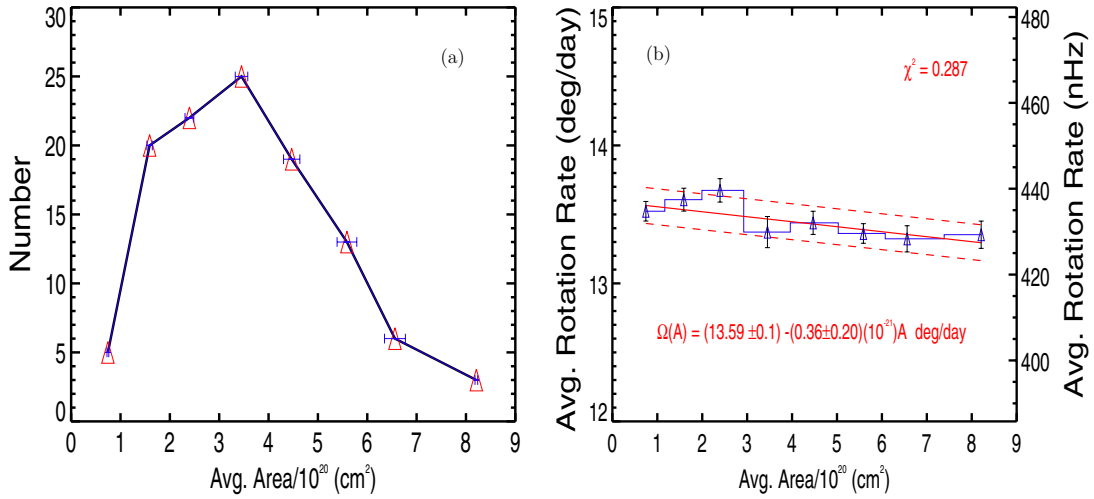

Figure 5. Irrespective of their latitude and number of days (τ) observed on the disk, for different area bins, panel (a) illustrates the occurrence number of CHs considered for the analysis, and panel (b) illustrates the variation of rotation rates for different average areas. In panel (b), the blue bar plot represents the computed rotation rates and the red continuous line represents a least-square fit $Y = a + bX$ to the observed values. Y is the observed rotation rate of the CH, X is the average area, and a and b are the constant coefficients determined from the least-square fit. The red dashed lines in panel (b) represent one standard deviation (which is computed from all the data points) error bands. χ^2 is a measure of goodness of fit.

(A color version of this figure is available in the online journal.)

each computed rotation rate of CHs, the respective latitude is assigned by averaging all the latitudes of CHs during its passage. As described in the previous paragraph, we binned the rotation rates and computed the average rotation rates, standard deviations, and error bars. For different latitude bins, the average rotation rates are subjected to a linear least-square fit and the results are presented in Figure 4. From both the rotation laws, compared to the first coefficient, the magnitude of the small second coefficient ($\Omega_d = -0.81(\pm 1.58)$ in Figure 3(a) or $\Omega_d = -0.51(\pm 1.64)$ in Figure 4(a)) suggests that *CHs rotate rigidly*.

As sunspots show different rotation rates for the small and big areas (Hiremath 2002), it is interesting to know whether similar variations in CH rotation rates exist. As CHs evolve, their area also changes and the question arises: for which area during the evolutionary passage does the rotation rate have to be considered? For this purpose, we adopt the following method: daily areas and rotation rates of CHs are computed. For all of the days of the existence of a CH, the average area and rotation rates are computed. Further, irrespective of their latitude and τ, rotation rates are collected for the area bins $(0\text{–}1)\times 10^{20}$ cm^2, $(1\text{–}2)\times 10^{20}$ cm^2, etc., and *mean rotation rates* are computed. In Figure 5(a), we present the occurrence number of CHs for different area bins, while, regardless of their latitudes and τ, for different area bins, Figure 5(b) illustrates the *mean rotation rates* of CHs. It is important to note from Figure 5(b) that, unlike sunspots, all of the CHs (as the second coefficient is almost zero, i.e., $(0.36 \pm 0.20) \times 10^{-21}$) *rotate rigidly*. This important result implies that all CHs must originate from the same region of the solar interior that rotate rigidly.

3.2. Average Rotation Rates: Variations with Respect to τ and Daily Evolution

In order to check the dependency of rotation rates of CHs with respect to the number of observed days τ, daily rotation rates are computed during their evolution. As described in Section 3, if a CH has τ of n days, we have $(n-1)$ rotation rates. Irrespective of their areas and the latitude, for each τ, rotation rates are collected and the average rotation rate is computed, the results of which are illustrated in Figure 6(a). We find that rotation rates of CHs are independent of τ.

Further, irrespective of their area and τ, we combine daily rotation rates for all the latitudinal bins and present the resulting daily average rotation rates in Figure 6(b). If CHs rotate rigidly and are independent of latitude, then the integrated rotation rates for all the latitudes should remain constant. For example, let us consider the rotation law (red continuous line) overplotted in Figure 6(b). From this law, when one computes the difference between rotation rates of the first day and the tenth day, the difference is found to be $\sim$0.1 deg day^{-1}. This is approximately the same magnitude as the formal uncertainty in the value for each bin, once again strongly suggesting that *CHs rotate rigidly, for all the days during their evolutionary passage.*

3.3. Comparison of the Rotation Rates of CHs with Other Activity Indices

Compared to the rotation rates obtained by other surface activity indices (Figures 7 and 8), (1) CHs rotate almost like a rigid body and (2) on average coronal holes rotate slower ($\sim$440 nHz) than the rotation rates of other activity indices over the latitude range -40 to $+40$. The ratio $R = |\Omega_d/\Omega_0|$ of the two coefficients of each rotational law gives a sense of whether the rotation is rigid or differential. For example, if one computes this ratio for sunspots ($R_{\rm sunspot}$) and for coronal holes ($R_{\rm coronal\_hole}$), it is clear that $R_{\rm sunspot} \gg R_{\rm coronal\_hole}$; this can also be seen from the fifth column of Table 2. In this table, goodness of fit χ^2 is also given in the last column. The small value of χ^2 (typically χ^2 should be $\leqslant (N-n)$, where N is the total number of data points and n is degrees of freedom, in this case $n = 2$) implies that the fit is very good. At least compared with any features lower in the solar atmosphere, it is clear that *CHs rotate rigidly*.

3.4. First Rotation Rates: Variations with Respect to Latitude and the Number of Observed Days τ

In the previous subsections, on the basis of the small magnitude of the second coefficient (as illustrated in Figures 3 and 4) in the rotation law and the ratio R of CH, we concluded that CHs rotate rigidly. Although the second coefficient is small, it is

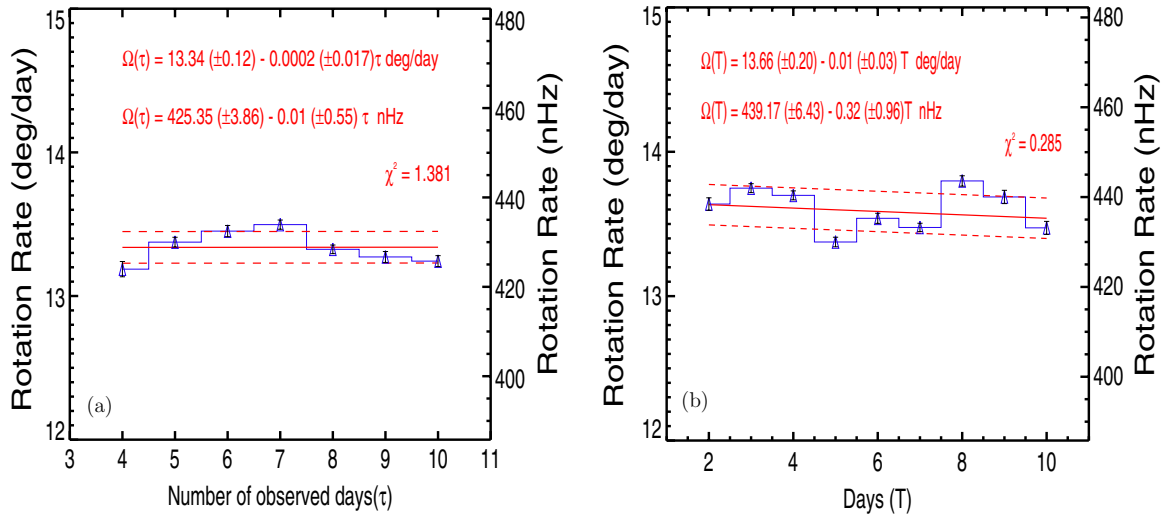

Figure 6. Irrespective of their area and latitude, panels (a) and (b) illustrate the variation of the rotation rates of CHs for different τ and for different days during their evolution, respectively. In both the figures, the blue bar plot represents the computed rotation rates and the red continuous line represents a least-square fit $Y = a + bX$ to the observed values. Y is the observed rotation rate of the CH, X is either τ or different days represented by T, and a and b are the constant coefficients determined from the least-square fit. The red dashed lines represent one standard deviation (which is computed from all the data points) error bands. χ^2 is a measure of goodness of fit.

(A color version of this figure is available in the online journal.)

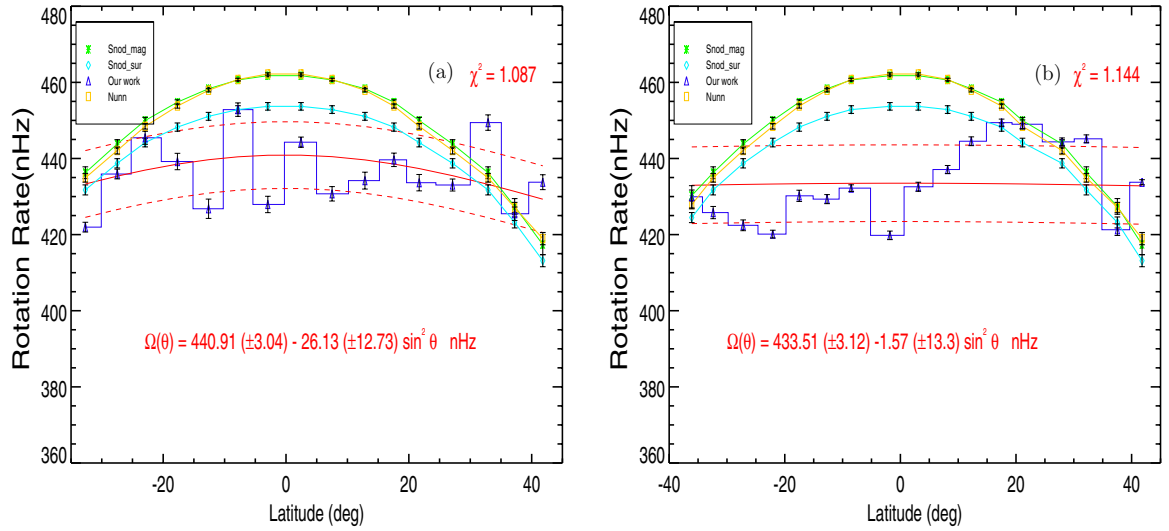

Figure 7. Irrespective of their areas, for different latitudes, blue bar plots connected by triangles in both the plots represent the rotation rates of CHs as determined from the first method (see Section 2). The blue bar plots in both the illustrations represent rotation rates of CHs that occur between east and west of 65° (a) and 45° (b) central meridian distances, respectively. The rotation rates of sunspots (yellow curve; Newton & Nunn 1951), magnetic activity (green curve; Snodgrass 1983), and surface rotation (cyan curve; Snodgrass 1992) are also overplotted. The red dashed lines in both the figures represent one standard deviation (which is computed from all the data points) error bands. χ^2 is a measure of goodness of fit.

(A color version of this figure is available in the online journal.)

not completely negligible to conclude unambiguously that CHs rotate rigidly, which means that a small contribution to the second coefficient due to differential rotation cannot be ruled out. This result can be interpreted as follows: the rotation rates of CHs presented in the previous sections are a combination of the rotation rates of CHs that are anchored at different parts of the interior during their evolutionary passage on the visible disk. That means if CHs originate only in the convective envelope and raise their anchoring feet toward the surface, owing to differentially rotating convection zone and similar to magnitudes of the rotation rates of sunspots, one should obtain a reliable and large magnitude of the second coefficient in the rotation law. On the other hand, if the CHs originate in the radiative core and raise their anchoring feet toward surface, during their first appearance on the surface, one should obtain combined contribution (from the differential and rigidly rotating regions) to the second coefficient. That means if one computes the *first rotation rates* Ω_1 of CHs during their first appearance on the surface for different latitudes and number of days (τ) observed on the disk, one should obtain an unambiguously negligible contribution from the second coefficient of the rotation law. In order to test this conjecture, the first rotation rates Ω_1 of CHs are computed as follows: again, we consider CH that are born between +65° and −65° from the central meridian. From the first- and second-day computed longitudes (from the central meridian) of CHs and by using first method, the *first rotation rates* are computed. Each *first rotation rate* is collected in 5° latitude bins, and the average of the first rotation rates is computed and, for different latitudes,

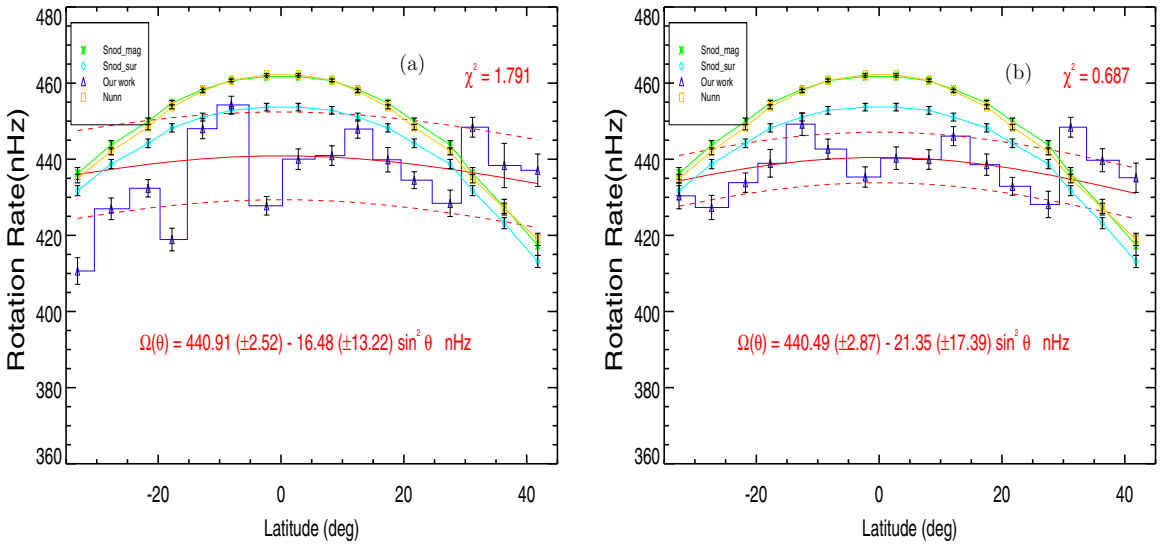

Figure 8. Irrespective of their areas, for different latitudes, the blue bar plots connected by triangles in both the plots represent the rotation rates of CHs as determined from the second method (see Section 3.1). The blue bar plots in both the illustrations represent rotation rates of CHs that occur between east and west of 65° (a) and 45° (b) central meridian distances, respectively. The rotation rates of sunspots (yellow curve; Newton & Nunn 1951), magnetic activity (green curve; Snodgrass 1983), and surface rotation (cyan curve; Snodgrass 1992) are also overplotted. The red dashed lines in both the figures represent one standard deviation (which is computed from all the data points) error bands. χ^2 is a measure of goodness of fit.

(A color version of this figure is available in the online journal.)

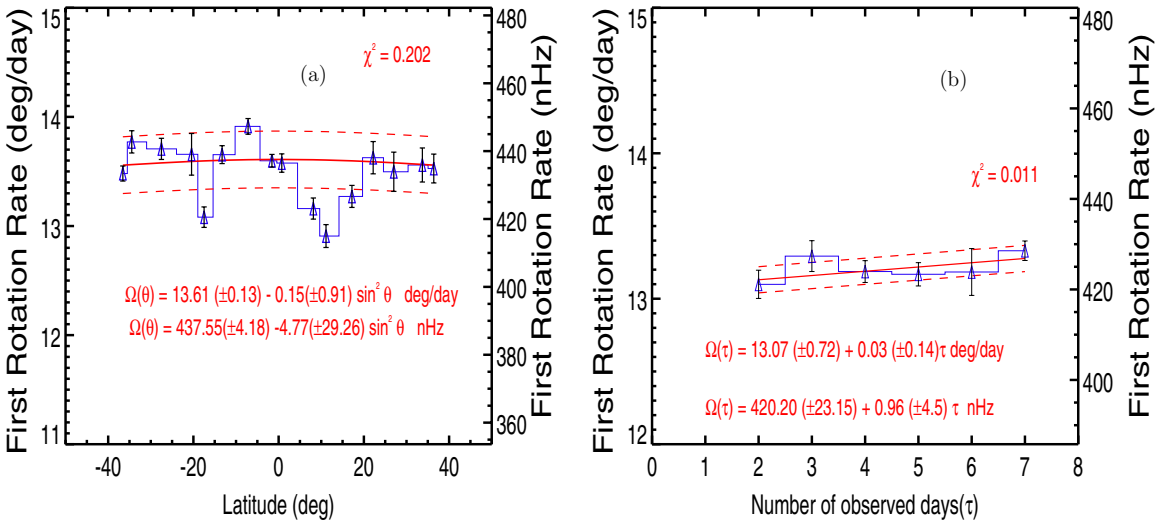

Figure 9. Irrespective of their area and the number of days (τ) observed on the disk, panel (a) illustrates the variation of first rotation rates of CH with respect to latitude. Irrespective of their area and latitude, for different τ, panel (b) illustrates the variation of first rotation rates of CHs. The red dashed lines in both the figures represent one standard deviation (which is computed from all the data points) error bands. χ^2 is a measure of goodness of fit.

(A color version of this figure is available in the online journal.)

are illustrated in Figure 9(a). Similarly, for different τ, the first rotation rates are collected and the average of the first rotation rates is computed and the results are presented in Figure 9(b). It is important to note that, according to our conjecture, we find that the magnitude of the second coefficient has a negligible contribution to the rotation law, which leads to the inevitable conclusion that *CH must rotate rigidly*.

From all of these results, finally we conclude unambiguously that, *independent of their area, the number of observed days (τ), and latitude, CHs rotate rigidly during the evolutionary passage on the solar disk*. However, it is interesting to note from the present and previous studies (Wagner 1975, 1976; Timothy & Krieger 1975; Bohlin 1977) that although whole coronal hole structure rotates rigidly, individual coronal bright points (CBP) embedded in CHs rotate differentially (Karachik et al. 2006). As pointed out by these authors, CBPs in the corona might be influenced by the surrounding differentially rotating plasma. However, it is not clear how CBPs are influenced by the differential rotation of the surrounding plasma.

4. DISCUSSION AND CONCLUSIONS

In contrast to other persistent solar features of the corona, then, why do CHs rotate rigidly? Many observations (Madjarska et al. 2004; Subramanian et al. 2010; Tian et al. 2011; Yang et al. 2011; Krista 2011; Krista et al. 2011; Crooker & Owens 2011; Madjarska et al. 2012) suggest magnetic reconnection at coronal hole boundaries (CHBs) as the cause of rigid body rotation.

Pevtsov & Abramenko (2010) conclude that the CH rotation rate is almost like the rotation rate of sunspots, and the CHs are

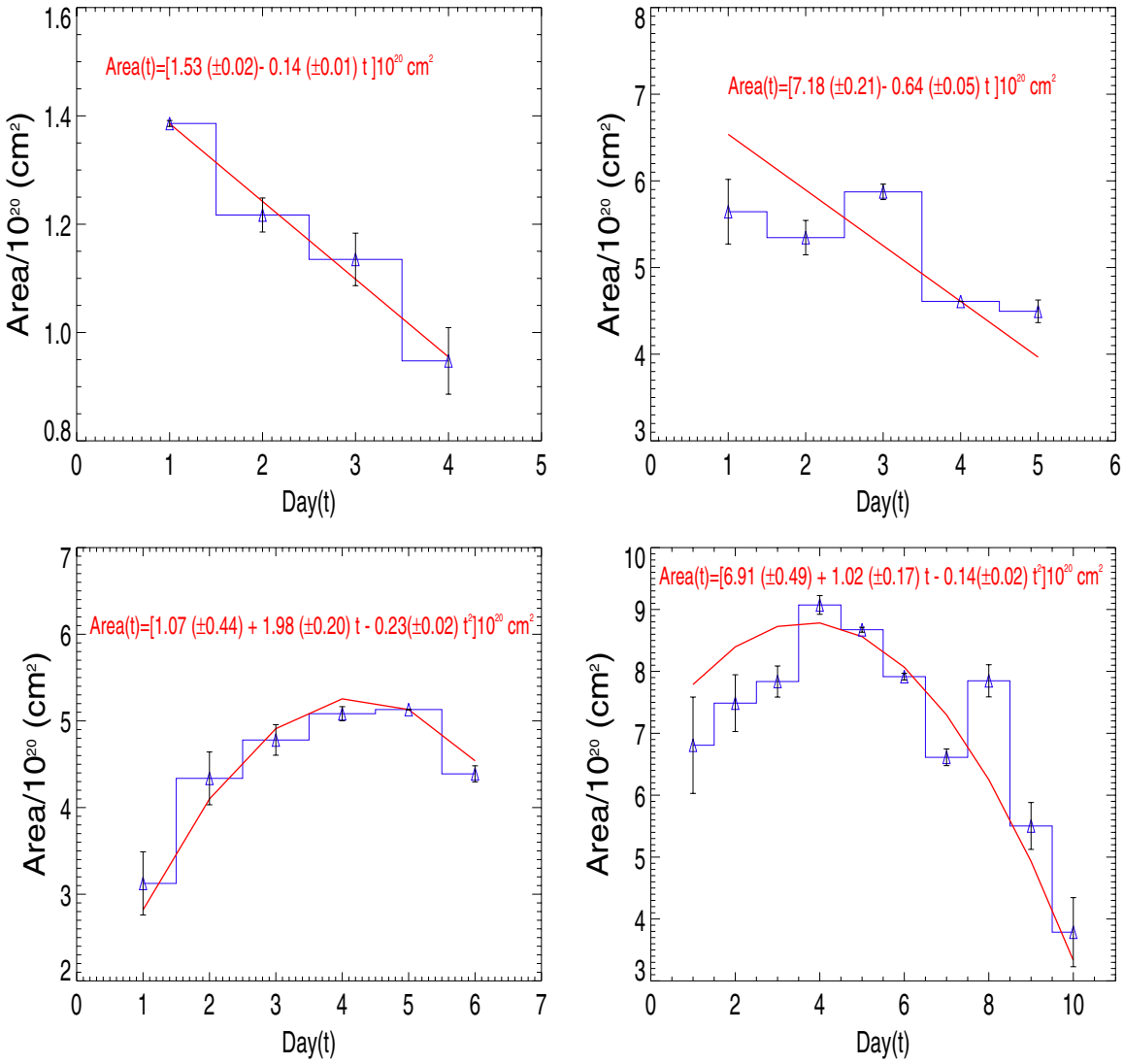

Figure 10. For different days, the measured average areas of the CH (blue bar plot) that are normalized with the area 10^{20} cm^2. The schematics in the upper panel are the variation of areas of CHs for the number of observed days (τ), which are 4 and 5, respectively, while the schematics in the lower panel illustrate the variation of areas of CHs for the number of observed days (τ), which are 6 and 10, respectively. χ^2 is a measure of goodness of fit.

(A color version of this figure is available in the online journal.)

"analogous to a grass fire, which supports itself by continuously propagating from one patch of dry grass to the other." That means a CH constantly changes its footprint, moving from one available polarity to another. This implies that the area of a CH will depend on the size of the available polarity footprint, and it can either decrease or increase depending on the size of the photospheric magnetic field patch. This also suggests that, on average, the difference in the coordinates at the eastern and western boundaries should remain constant, yielding a rigid body rotation rate (as suggested by previous studies). Thus, one can argue that CHs are surface phenomena. If the CH is a surface phenomenon and if it constantly changes its footprint by moving from one available polarity to other, the area of CH depends on the size of the available polarity footprint. Hence, the area should either decrease or increase with a result that, on average, area with respect to time must be nearly constant. In order to test this conjecture, in Figure 10 we illustrate measured areas (that are corrected for projection) of CHs that have τ of 4 days and 5 days (upper panel), and 6 days and 10 days (lower panel), respectively. The dates of the occurrences of these individual CHs presented in the upper panel are 2001 November 6 to November 9 (2° to 41° east of central meridian) and 2004 May 8 to May 12 (30° east to 12° west of central meridian). The dates of the occurrences of CHs that are presented in the lower panel are 2003 August 21 to August 26 (45° east to 11° west of central meridian) and 2005 December 22 to December 31 (50° east to 62 ° west of central meridian).

One can notice from Figure 10 that, contrary to the expectation that CH area nearly remains constant during its evolution, on average, the area of CHs smoothly decreases (upper panel) continuously or increases like sunspots' area evolutionary curve, reaches maximum area, and then smoothly decreases (lower panel). From these figures, we cannot find other expected signatures for the reconnection, viz. substantial daily variations of areas of CHs during their evolution. This does not mean that there is no magnetic reconnection at the boundaries. However, in the following, we show that magnetic reconnection alone cannot sufficiently explain the dynamics (rigid body rotation) and area evolution of CHs. Hence, CHs must be deep rooted rather than mere surface phenomena. Interestingly, similar to Bohlin's

Table 2
Sidereal Rotation Rates (deg day^{-1}) Obtained by the Present and Previous Studies

Different Regions	Observations	Wavelength Region	Coefficients Ω_0	Coefficients Ω_d	$\lvert\Omega_d/\Omega_0\rvert$	χ^2
Corona	Coronal holes[1]	EUV	13.71	−0.81	0.059	1.086
Corona	Coronal holes[1a]	EUV	13.48	−0.05	0.004	1.144
Corona	Coronal holes[2]	EUV	13.71	−0.51	0.037	1.791
Corona	Coronal holes[2a]	EUV	13.70	−0.66	0.048	0.686
Corona	Coronal holes[3]	EUV	13.61	−0.15	0.011	0.202
Photosphere	Doppler shift[4]	Visible	14.11	−1.70	0.121	
Photosphere	Surface magnetic[5]	Visible	14.37	−2.30	0.160	
Photosphere	Sunspots[6]	Visible	14.38	−2.96	0.206	
Photosphere	Sunspots[7]	Visible	14.37	−2.59	0.180	
Radiative Core	Helioseismic[8]		13.63	−0.64	0.047	5.401

Notes.
[1] Average rotation rates from the first method and for the CMD (+65° to −65°).
[1a] Average rotation rates from the first method and for the CMD (+45° to −45°).
[2] Average rotation rates from the second method and for the CMD (+65° to −65°).
[2a] Average rotation rates from the second method and for the CMD (+45° to −45°).
[3] First rotation rates for the CMD (+45° to −45°).
[4] Snodgrass (1992).
[5] Snodgrass (1983).
[6] Newton & Nunn (1951).
[7] Brajša et al. 2002.
[8] Antia & Basu (2010).
* CMD: central meridian distance.

(1977) study, we also find the same order ($\sim 10^{14}$ cm^2 s^{-1}) of average growth (or decay) of CHs.

One would also expect that magnetic reconnection at the CH boundary might substantially contribute to the enhancement of the average intensity (DN counts). In order to check this expectation, for the same CH presented in Figure 10, we compute the daily average DN counts ($= \sum_{i=1}^{n} \mathrm{DN}_i/N$, where N is the total number of pixels), which are illustrated in Figure 12. The obvious fact from Figures 10 and 12 is that as the area of CHs increases, average DN counts (intensity) decrease and vice versa. However, according to our expectation, CHs do not show any transient and substantial increase in intensity during their daily evolutionary passage on the solar disk.

Of course, as CHs are embedded in the atmosphere where closed field lines due to active regions coexist, it is natural to expect reconnection at the boundary of a CH due to oppositely directed field lines. The possible reason for the null detection of magnetic reconnection from our data set is the low temporal resolution of daily data used in this analysis. In fact, with a high temporal resolution of the CH data set, a majority of previous studies (Wang et al. 1998; Madjarska et al. 2004, 2012; Raju et al. 2005; Aiouaz 2008; Madjarska & Wiegelmann 2009; Subramanian et al. 2010; Edmondson et al. 2010; Krista 2011; Yang et al. 2011) show evidence of reconnection, although other studies lack such evidence (Kahler & Hudson 2002; Kahler et al. 2010). If we follow the majority of the results that the rigid rotation rates of the CHs are due to the magnetic reconnection at the CHBs, then one would expect that the area of the CHs during their disk passage must remain constant. As most of these majority of studies used short (∼hours) duration data sets, the question arises whether CHs maintain their areas throughout disk passage (as one can see from our analysis, most of CHs exist for more than five days on the solar disk). One can notice from the area–time plots (Figure 10), during (∼days) its disk passage, CHs do not maintain their areas and hence their rigid body rotation rate is not due to interchange reconnection. As the previous studies use high-temporal, short-duration (∼hours) data sets, and during such timescales (as the CH has a large dimension) obviously one gets constant shape, and therefore a conclusion that rigid rotation rates of CHs are due to magnetic reconnection. However, we stress from the results presented in Figure 10 that, on long duration (>5 days), CHs do not maintain their shape and the rigid body rotation rate of CHs is not due only to magnetic reconnection at their boundaries. The rigid body rotation rate of CH is likely due to the deep rooted anchoring of the feet and subsequent raise toward the surface and then to the atmosphere.

As for the area evolution of the CH, the question arises as to which is the dominant physical process that dictates temporal variation of area, and hence removal of magnetic flux of the CH? Is it due to *magnetic diffusion* (whose diffusion timescale is $\sim L/\eta^2$) or *magnetic reconnection* at the CHBs? Similar to sunspots' area evolution curve (Hiremath 2010a, 2010b), the formation and growth parts of area evolution of CHs are not understood. However, in order to answer the aforementioned queries, we consider decay part of the area evolution curve for the following two physical reasons: (1) if area evolution of CHs is dominated by magnetic diffusion, then its area must vary $\sim t^{-1/2}$ (where t is the time variable), and (2) if area evolution of CHs is mainly due to magnetic reconnection, annihilation of magnetic flux due to the reconnection of the opposite magnetic field lines at the boundaries of the CH leads to an exponential decrease of area with time. If the CH is considered to be magnetic flux tube with uniform magnetic field structure, from magnetic induction equation (with diffusive-dominated term), it is instructive to show that the equation for the rate of change of magnetic flux ϕ is $(d\phi/dt) = \eta(d^2\phi/dr^2)$ (where $\phi = \int_0^r B_z A dr$ is the magnetic flux of the CH flux tube, $A(= 2\pi r)$ is the area, t is the time variable, η is the magnetic diffusivity, B_z is a uniform magnetic field structure along the z-direction, and r is the radius of the flux tube). From the results (Krista & Gallagher 2009; CHARM algorithm from www.solarmonitor.org) illustrated in Figure 11(a), the absolute magnitude of B_z of 10 days CH (during the decay part of its area evolution as presented in Figure 10) is found to be nearly independent of time (number of observed days). Using this observational information and assumption that the magnetic field structure of CHs is also uniform spatially along the r-direction, it can be easily shown from the rate of change of the magnetic flux equation that $(dA/dt) = \eta(d^2A/dr^2)$, the solution of which is obtained as $A \sim t^{-1/2}$ on diffusion timescales.

In order to test these aforementioned two reasonings, the decay part of 10 days area evolution curve is subjected to diffusion and exponential fits. After linearizing the two laws, least-square fits are performed and the result is illustrated in Figure 11(b). Compared to the exponential fit, for the decay part of the area evolution curve, least-square fit for the law of diffusion yields a very low value of χ^2 with an expected decay index of ∼−0.5. Hence, during the decay part of its evolution of area, CHs are consistent with the first reasoning and area evolution of CHs is mainly dictated by magnetic diffusion. However, persistent magnetic reconnection at the boundaries of CHs during their evolution cannot be neglected. Thus, it is reasonable to conclude that *both the magnetic diffusion and the reconnection processes control the evolution of the area of CHs during their passage on the solar disk.*

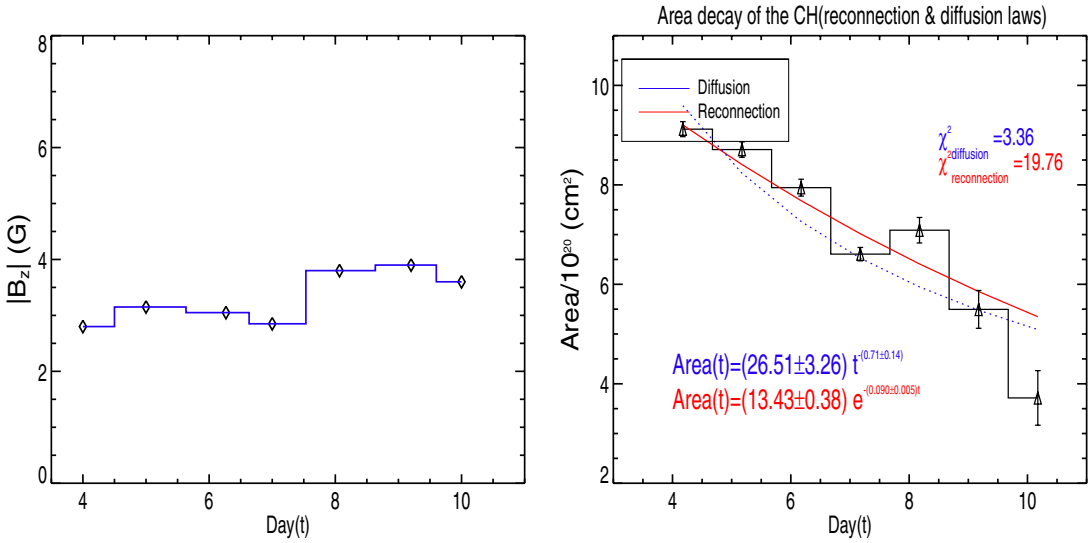

Figure 11. Variation of absolute magnitude of the magnetic field structure (blue bar plot connected by diamonds; left figure) and area (black bar plot connected by triangles; right figure) of a CH for the decay part of 10 days area evolutionary curve. Areas are normalized with the area 10^{20} cm^2 and are subjected to the laws of magnetic diffusion (area$(t) = A_0 t^{-n}$, t is the time variable) and magnetic reconnection (area$(t) = A_0 e^{-c_1 t}$), respectively. A_0, constants n, and c_1 are determined from the least-squares fit. χ^2 is a measure of goodness of fit.

(A color version of this figure is available in the online journal.)

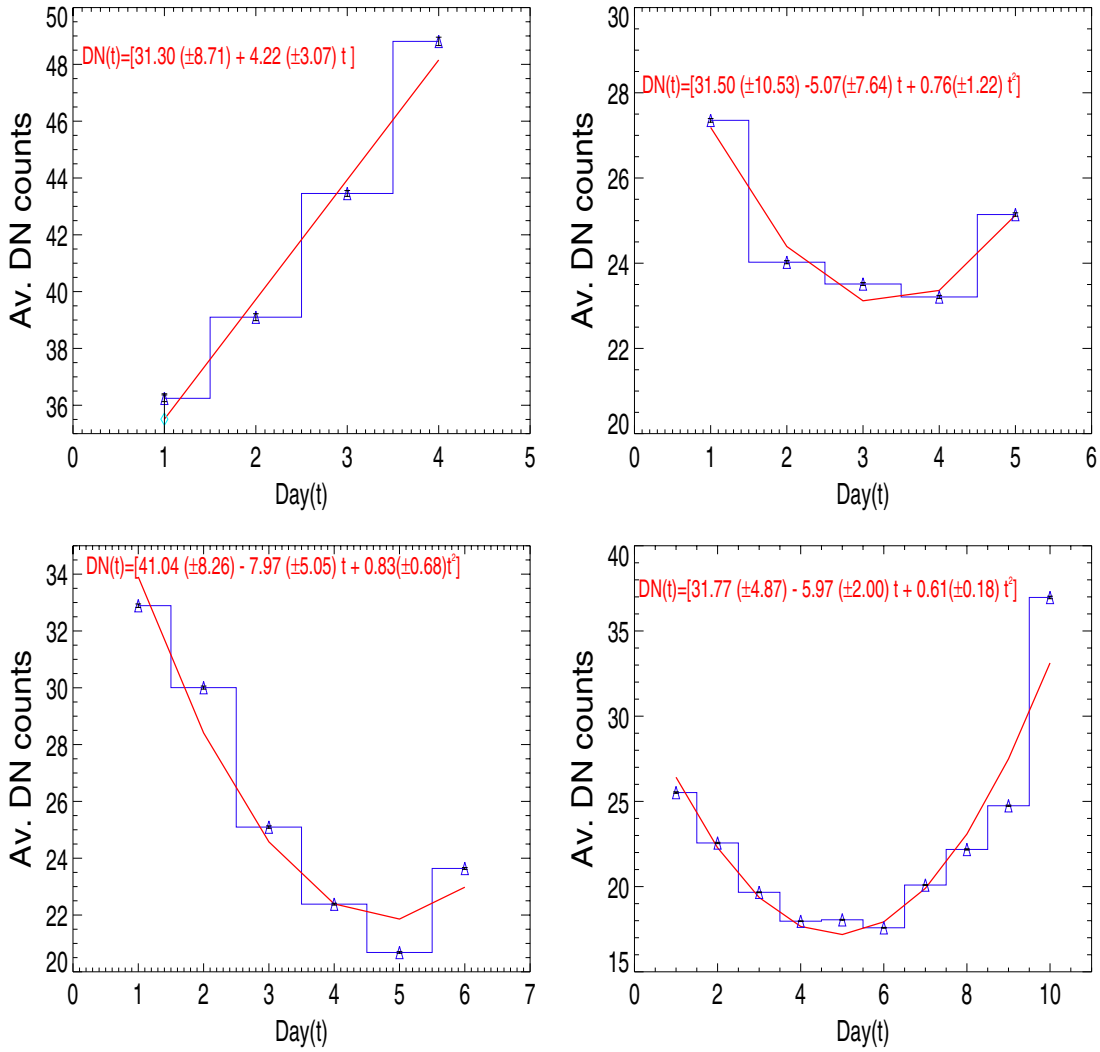

Figure 12. For different days, measured average DN counts of CHs (blue bar plot). The schematics in the upper panel are the variation of average DN counts of CHs for the number of observed days (τ), which are 4 and 5, respectively, while the schematics in the lower panel illustrate variation of average DN counts of CH for number of observed days (τ), which are 6 and 10, respectively.

(A color version of this figure is available in the online journal.)

Another important result from this study is an explanation of why CHs rotate with a magnitude of ∼438 nHz during their first appearance, whereas other active regions, approximately at the same height in the corona, have a magnitude of the rotation rate similar to the rotation rate of sunspots. Moreover, similar to sunspots, CHs are likely to be three-dimensional structures whose dynamical evolution is not only controlled by the surface activity, but also related to the solar interior dynamics where roots of CH might be anchored, probably below the base of the convection zone. The idea that CHs probably originate below the base of the convection zone is not a new one. In fact, nearly three decades ago, Gilman (1977) came to the conclusion that CH origin and formation may not be due to the so-called dynamo mechanism that apparently explains the genesis of the sunspot cycle. While discussing the origin of XBP (X-ray bright points), Golub et al. (1981) came to the conclusion that XBP and CHs probably originate below the base of the convection zone. Recently, Jones (2005) also expressed similar doubts about the origin of CHs and concluded that their roots must be deeper below the base of the convection zone. Very recently, by investigating the formation of isolated, non-polar CHs on the remnants of four decaying active regions at the minimum/early ascending phase of sunspot activity, Karachik et al. (2010) came to a similar conclusion that during their first appearance CH might be deeply rooted.

Hence, on the basis of these two important results ((1) first rotation rates of CH during their initial appearance and during evolutionary passage and (2) magnitude of rotation rates (∼438 nHz)), we suggest a possibly naive but reasonable proposition in the following way: compared to other activity indices such as X-ray bright points (XBP), CHs are very large (∼10 times the typical big sunspot), and it is not unreasonable to suggest that their roots may be anchored very deep below the surface. In the case of coronal XBP, from the nature of their differential rotation rates, Hara (2009) has conjectured that their roots might be anchored in the convective envelope, as helioseismic inferences (Antia et al. 1998; Antia & Basu 2010) show that the whole convective envelope is rotating differentially. On the other hand, the present and previous studies (Wagner 1975; Wagner 1976; Timothy & Krieger 1975; Bohlin 1977) strongly suggest that the rotation rate of CHs is independent of latitude, number of days (τ) observed on the disk, and area.

As for the anchoring depths, during CHs' first appearance in the corona and owing to its magnetic nature (Gurman et al. 1974; Bohlin 1977; Levine 1977; Bohlin & Sheeley 1978; Stenflo 1978; Harvey & Sheeley 1979; Harvey et al. 1982; Shelke & Pande 1984; Obridko & Shelting 1989; Zhang et al. 2006; Fainshtein et al. 2010) , we expect that a CH might isorotate with the solar plasma, so its rotation rate during its first appearance and the rotation rate at the anchoring depth must be identical. It is interesting to note that the average rotation rate (∼438 nHz) we have measured in CHs (Figure 13) is similar to that of the average rotation rate of the solar plasma inferred by helioseismology (Antia & Basu 2010; rotation rate of the solar interior averaged over one solar cycle is kindly provided by Prof. Antia) at a depth of ∼0.62(±0.10) $R_\odot$. Hence, during the first CHs' appearance, it is reasonable to suggest that the depth of anchoring of CH might be around 0.62(±0.10) $R_\odot$. If we simply identify the rotation rates found here with the internal rotation rate at a given depth, we find a match only inside the radiative interior at a depth of 0.62(±0.10) $R_\odot$ solar radii. In the future, helioseismology may give further inferences on the anchoring depths of CHs.

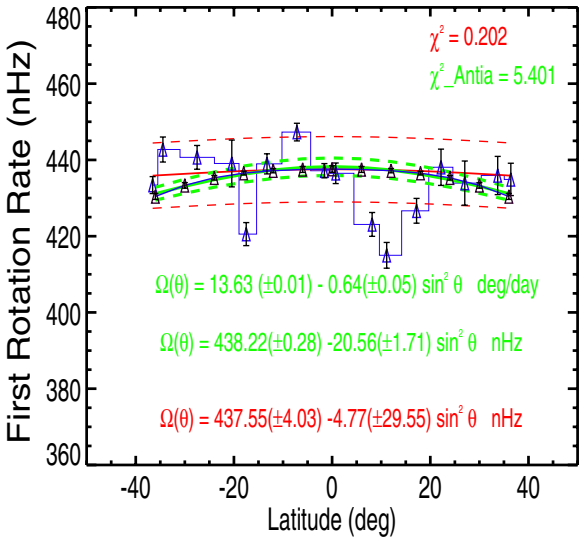

Figure 13. For all the sizes and number of observed days (τ), this figure illustrates first rotation rates of CHs (blue bar plot connected by blue triangles) with a least-square fit (red continuous line). Also plotted is the helioseismically inferred (Antia & Basu 2010) rotation rate (green continuous line connected by black triangles with green dashed lines as one sigma error band) at a depth of 0.62(±0.10) $R_\odot$, as a function of latitude. The red and green dashed lines represent one standard deviation (that is computed from all the data points) error bands. χ^2 is a measure of goodness of fit.

(A color version of this figure is available in the online journal.)

We know, however, of no currently accepted model of magnetic field generation that could anchor coronal structures to such a depth in the interior. Unless a consistent and acceptable theoretical model of CHs that supports of our proposition (that during their first appearance, roots of CH might be anchored in the radiative core), our proposed idea remains mere a conjecture only.

To conclude this study, we used *SOHO*/EIT 195 Å calibrated images to determine the latitudinal and day-to-day variations of the rotation rates of CHs. We found that (1) irrespective of their areas and number of days (τ) observed on the disk, for different latitude zones, the rotation rates of CHs follow a rigid body rotation law; (2) CHs also rotate rigidly during their evolution history; and (3) during their first appearance, CHs rotate rigidly with a constant angular velocity ∼438 nHz that only matches depth around 0.62(±0.10) $R_\odot$ in the radiative interior. This result is so counterintuitive that we can only conclude that we do not understand why CHs rotate rigidly at that rate.

The authors are grateful to the anonymous referee for the invaluable comments and suggestions that substantially improved the results and presentation of the manuscript. The authors are also grateful to Dr. J. B. Gurman for giving useful information on the *SOHO* data, for going through an earlier version of this manuscript, and for giving useful ideas. Hiremath is thankful to the former Director, Prof. Siraj Hasan, Indian Institute of Astrophysics, for encouraging this ISRO funded project. This work has been carried out under "CAWSES India Phase-II program of Theme 1" sponsored by Indian Space Research Organization(ISRO), Government of India. *SOHO* is a mission of international cooperation between ESA and NASA.

REFERENCES

Aiouaz, T. 2008, ApJ, 674, 1144
Antia, H. M., & Basu, S. 2010, ApJ, 720, 494

Antia, H. M., Basu, S., & Chitre, S. M. 1998, MNRAS, 298, 543
Balthasar, H., Vazquez, M., & Woehl, H. 1986, A&A, 155, 87
Bohlin, J. D. 1977, SoPh, 51, 377
Bohlin, J. D., & Sheeley, N. R., Jr. 1978, SoPh, 56, 125
Brajša, R., Wöhl, W., Vršnak, B., et al. 2002, SoPh, 206, 229
Brajša, R., Wöhl, W., Vršnak, B., et al. 2004, A&A, 414, 707
Chandra, S., Vats, H. O., & Iyer, K. N. 2009, MNRAS, 400, L34
Chandra, S., Vats, H. O., & Iyer, K. N. 2010, MNRAS, 407, 1108
Choi, Y., Moon, Y.-J., Choi, S., et al. 2009, SoPh, 254, 311
Cranmer, S. R. 2009, LRSP, 6, 3
Crooker, N. U., & Owens, M. J. 2011, SSRv, 172, 201
Dalsgaard, C. J., & Schou, J. 1988, in Seismology of the Sun and Sun-like Stars, ed. E. J. Rolfe (ESASP 286; Noordwijk: ESA), 149
Delaboudiniére, J. P., Artzner, G. E., Brunaud, J., et al. 1995, SoPh, 162, 291
de Toma, G. 2011, SoPh, 274, 195
Edmondson, J. K., Antiochos, S. K., DeVore, C. R., Lynch, B. J., & Zurbuchen, T. H. 2010, ApJ, 714, 517
Fainshtein, V. G., Stepanian, N. N., Rudenko, G. V., Malashchuk, V. M., & Kashapova, L. K. 2010, BCrAO, 106, 1
Fisher, R., & Sime, D. G. 1984, ApJ, 287, 959
Freeland, S. L., & Handy, B. N. 1998, SoPh, 182, 497
Gilman, P. A. 1977, in Coronal Holes and High Speed Wind Streams Conference, ed. J. B. Zirker (Boulder, CO: Associated Univ. Press), 331
Golub, L., Rosner, R., Vaiana, G. S., & Weiss, N. O. 1981, ApJ, 243, 309
Gurman, J. B., Withbroe, G. L., & Harvey, J. W. 1974, SoPh, 34, 105
Hansen, R. T., Hansen, S. F., & Looms, H. G. 1969, SoPh, 10, 135
Hara, H. 2009, ApJ, 687, 980
Harvey, J. W., & Sheeley, N. R., Jr. 1979, SSRv, 23, 139
Harvey, K. L., Harvey, J. W., & Sheeley, N. R., Jr. 1982, SoPh, 79, 149
Hiremath, K. M. 2002, A&A, 386, 674
Hiremath, K. M. 2009, SunGe, 4, 16
Hiremath, K. M. 2010a, SunGe, 5, 17
Hiremath, K. M. 2010b, arXiv:1012.5706
Hoeksema, J. T. 1984, PhD thesis, Stanford Univ.
Howard, R., Gilman, P. I., & Gilman, P. A. 1984, ApJ, 283, 373
Howard, R., & Harvey, J. 1970, SoPh, 12, 23
Howard, R., & La Bonte, B. J. 1980, ApJL, 239, 33
Howe, R. 2009, LRSP, 6, 1
Insley, J. E., Moore, V., & Harrison, R. A. 1995, SoPh, 160, 1
Javaraiah, J. 2003, SoPh, 212, 23
Jones, H. P. 2005, in ASP Conf. 346, Large-scale Structures and their Role in Solar Activity, ed. K. Sankarasubramanian, M. Penn, & A. Pevtsov (San Francisco, CA: ASP), 229
Kahler, S. W., & Hudson, H. S. 2002, ApJ, 574, 467
Kahler, S. W., Jibben, P., & Deluca, E. E. 2010, SoPh, 262, 135
Karachik, N. V., & Pevtsov, A. A. 2011, ApJ, 735, 47
Karachik, N. V., Pevtsov, A. A., & Abramenko, V. I. 2010, ApJ, 714, 1672
Karachik, N. V., Pevtsov, A. A., & Sattarov, I. 2006, ApJ, 642, 562
Kariyappa, R. 2008, A&A, 488, 297
Komm, R. W., Howard, R. F., & Harvey, J. W. 1993, SoPh, 145, 1
Krieger, A. S., Timothy, A. F., & Roelof, E. C. 1973, SoPh, 29, 505
Krista, L. D. 2011, PhD thesis, Trinity College, Univ. Dublin
Krista, L. D., & Gallagher, P. T. 2009, SoPh, 256, 87
Krista, L. D., Gallagher, P. T., & Bloomfield, D. S. 2011, ApJ, 731, 26
Lei, J., Thayer, J. P., Forbes, J. M., Sutton, E. K., & Nerem, R. S. 2008, GRL, 35, L19105
Levine, R. H. 1977, ApJ, 218, 291
Li, K. J., Shi, X. J., Feng, W., et al. 2012, MNRAS, 423, 3584
Madjarska, M. S., Doyle, J. G., & van Driel-Gesztelyi, L. 2004, ApJL, 603, 57
Madjarska, M. S., Huang, Z., Doyle, J. G., & Subramanian, S. 2012, A&A, 545, A67
Madjarska, M. S., & Wiegelmann, T. 2009, A&A, 503, 991
Mancuso, S., & Giordano, S. 2011, ApJ, 729, 79
Navarro-Peralta, P., & Sanchez-Ibarra, A. 1994, SoPh, 153, 169
Neupert, W. M., & Pizzo, V. 1974, JGR, 79, 3701
Newton, H. W., & Nunn, M. L. 1951, MNRAS, 111, 413
Nolte, J. T., Krieger, A. S., Timothy, A. F., et al. 1976, SoPh, 46, 303
Parker, G. D., Hansen, R. T., & Hansen, S. F. 1982, SoPh, 80, 185
Pevtsov, A. A., & Abramenko, V. I. 2010, in IAU Symp. 264, Solar and Stellar Variability: Impact on Earth and Planets, ed. A. G. Kosovichev, A. H. Andrei, & J.-P. Rozelot (Cambridge: Cambridge Univ. Press), 210
Obridko, V. N., & Shelting, B. D. 1989, SoPh, 124, 73
Raju, K. P., Bromage, B. J. I., Chapman, S. A., & Del Zanna, G. 2005, A&A, 432, 341
Ram, S. T., Liu, C. H., & Su, S.-Y. 2010, JGR, 115, 14
Roša, D., Brajša, R., Vršnak, B., & Wöhl, H. 1995, SoPh, 159, 393
Shelke, R. N., & Pande, M. C. 1984, BASI, 12, 404
Shelke, R. N., & Pande, M. C. 1985, SoPh, 95, 193
Shivaraman, K. R., Gupta, S. S., & Howard, R. F. 1993, SoPh, 146, 2
Shugai, Yu. S., Veselovsky, I. S., & Trichtchenko, L. D. 2009, Ge&Ae, 49, 415
Snodgrass, H. B. 1983, ApJ, 270, 288
Snodgrass, H. B. 1992, in ASP Conf. Ser. 27, The Solar Cycle, ed. K. L. Harvery (San Francisco, CA: ASP), 205
Snodgrass, H. B., & Ulrich, R. K. 1990, ApJ, 351, 309
Sojka, J. J., McPherron, R. L., van Eyken, A. P., et al. 2009, GeoRL, 36, L19105
Soon, W., Baliunas, S., Posmentier, E. S., & Okeke, P. 2000, NewA, 4, 563
Stenflo, J. O. 1978, RPPh, 41, 865
Subramanian, S., Madjarska, M. S., & Doyle, J. G. 2010, A&A, 516, A50
Thompson, M. J., Dalsgaard, C. J., Miesch, M. S., & Toomre, J. 2003, A&ARv, 41, 599
Thompson, M. J., Toomre, J., Anderson, E. R., et al. 1996, Sci, 272, 1300
Tian, H., McIntosh, S. W., Habbal, S. R., & He, J. 2011, ApJ, 736, 130
Timothy, A. F., & Krieger, A. S. 1975, SoPh, 42, 135
Ulrich, R. K., Boyden, J. E., Webster, L., & Shieber, T. 1988, in Seismology of the Sun and Sun-Like Stars, ed. E. J. Rolfe (ESASP 286; Noordwijk: ESA), 325
Verbanac, G., Vršnak, B., Veronig, A., & Temmer, M. 2011, A&A, 526, 20
Wagner, W. J. 1975, ApJL, 198, 141
Wagner, W. J. 1976, in IAU Symp. 71, Basic Mechanisms of Solar Activity, ed. V. Bumba & J. Kleczek (Cambridge: Cambridge Univ. Press), 41
Wang, Y. M. 2009, SSRv, 144, 383
Wang, Y. M., Sheeley, N. R., Jr., Nash, A. G., & Sampine, L. R. 1988, ApJ, 327, 427
Wang, Y. M., Sheeley, N. R., Jr., Socker, D. G., et al. 1998, ApJ, 508, 899
Weber, M. A., Acton, L. W., Alexander, D., Kubo, S., & Hara, H. 1999, SoPh, 189, 271
Weber, M. A., & Sturrock, P. A. 2002, in Multi-Wavelength Observations of Coronal Structure and Dynamics, Yohkoh 10th Anniversary Meeting, ed. P. C. H. Martens & D. Cauffman (New York: Elsevier), 347
Wilcox, J. M., & Howard, R. 1970, SoPh, 13, 251
Wittmann, A. D. 1996, SoPh, 168, 211
Wöhl, H., Brajša, R., Hanslmeier, A., & Gissot, S. F. 2010, A&A, 520, 29
Yang, S.-H., Zhang, J., Li, T., & Liu, Y. 2011, ApJL, 732, 7
Zhang, J., Jun, M., & Wang, H. 2006, ApJ, 649, 464
Zirker, J. B. 1977, RvGSP, 15, 257